Loss of Specular Reflection Due to Nonlinear Crack-Face Interaction

J. D. Achenbach and A. N. Norris¹

Received August 1, 1983; revised October 10, 1983

The interaction between rough crack faces is modeled by nonlinear relations between the crack-face tractions and the crack-opening displacements. These relations account for crack closure and for the related resistance to crack-face sliding. The relations are used to investigate reflection and transmission of an incident pulse by an infinite flaw plane. The problem statement is reduced to a set of inhomogeneous nonlinear ordinary differential equations for the displacement discontinuities, [u] and [v], across the flaw plane. These equations have been solved numerically. The reflected and transmitted displacement pulses follow directly from [u] and [v]. Next the Kirchhoff approximation in the time domain has been used to derive expressions for the specular reflection and transmission of an incident pulse by a crack with interacting crack faces. Both incident longitudinal and transverse waves have been considered. The loss of specular reflection as compared to a perfect (traction-free) crack is exhibited by specific examples.

KEY WORDS: Crack-opening displacement; crack closure; ultrasonics; Kirchoff approximation; NDE.

1. INTRODUCTION

A crack is a surface of displacement discontinuity. The failure processes that result in a crack generally produce rough crack faces. Once crack opening has taken place, and the crack faces have undergone the slightest relative sliding displacement, the crack will never completely close again due to incompatibility of the rough crack faces. Under subsequent loading conditions the faces of the crack generally are not free of surface tractions, as is assumed for a perfect mathematical crack, nor will there be perfect contact between the crack faces. Unless the crack faces are completely separated, a complicated interaction between the crack faces is to be expected, which will be different for opening and closing of the crack on the one hand, and relative sliding of the crack faces on

The effects of interaction between contacting crack faces are of particular interest in studies of crack detection and crack characterization by the use of the specular reflection and scattering of ultrasonic waves. A perfect mathematical crack acts as a perfect screen for reflection and scattering. It may be assumed that scattering results for the perfect mathematical crack-model are valid for a real crack if the amplitude of the incident wave is smaller than the average crack-opening displacement prior to wave incidence, and if the wavelength is much larger than a characteristic length of the roughness of the crack faces.

A crack with interacting crack faces may be a poor reflector, and thus difficult to detect and to characterize. In this paper we investigate the loss of

the other. The interaction of the crack faces will generally be a nonlinear process which will depend strongly on the magnitudes of the tractions transmitted across the contacting crack faces.

¹The Technological Institute, Northwestern University, Evanston, Illinois 60201.

specular reflection due to transmission across the crack faces by nonlinear crack-face interactions. The crack is represented by a flaw plane of traction continuity (the tractions may vanish) but possible displacement discontinuity. The interaction between the crack faces is described by nonlinear relations across the flaw plane between averaged tractions and averaged displacement discontinuities and their derivatives.

The effects of crack-face roughness and crackface interactions on the scattering of ultrasonic waves have been of concern to several investigators. Analytical studies have been presented by Haines, (1) Thompson et al., (2) and Buck et al. (3) The approach of the present paper is comparable to the one of Ref. (2), except that we take into account both normal and shear tractions across the flaw plane. In addition, the emphasis in the present paper is on cracks that are lightly closed and may experience separation of the crack faces as well as further closure. Since the resistance to crack closure is very different from the resistance to crack opening, the problem is then inherently nonlinear. If the crack should remain closed at all times a local perturbation about the closed state can be used as described in Ref. (2), to yield a linear problem statement. The postulated nonlinear flaw-plane relations used in this page contain a number of parameters which must be determined experimentally. Experimental investigations have been carried out by Woolridge^(4,5) and Golan,⁽⁶⁾ as well as by Thompson, et al. (2) An analytical study which takes into account nonlinear interaction effects at an interface for a one-dimensional configuration has been presented by Richardson. (7)

2. CONDITIONS AT THE FLAW PLANE

A schematical depiction of a flaw surface is shown in Fig. 1 (a). In this paper it is assumed that for the purpose of computing the fields of stress and deformation elsewhere in the body, the interaction between the upper and lower faces of the flaw plane can be described by appropriate relations between the tractions and displacement across a perfectly flat surface. This surface, which is shown in Fig. 1 (b), may be considered as the median plane of the actual flaw surface.

In the analytical model we consider averaged tractions and averaged displacement discontinuities per unit area, with respect to coordinates in the flaw

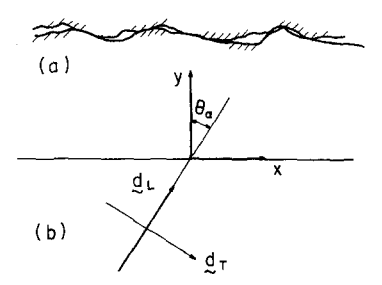


Fig. 1. Schematic depiction of flaw plane.

plane. The averaged tractions are continuous, which implies that at y = 0:

$$\sigma_{y}^{+} = \sigma_{y}^{-} = \sigma_{y}^{*}, \qquad \sigma_{yx}^{+} = \sigma_{yx}^{-} = \sigma_{yx}^{*}$$
 (1)

where the + and - signs refer to the upper and lower sides of the flaw plane as shown in Fig. 1 (b). It should be noted that Eq. (1) includes the conditions for a perfect mathematical crack, which are

$$\sigma_{y}^{+} = \sigma_{y}^{-} = 0, \qquad \sigma_{yx}^{+} = \sigma_{yx}^{-} = 0$$
 (2)

In the present model for a crack with rough crack faces, Eq. (1) will be supplemented by relations between the stresses σ_y^* , σ_{yx}^* and the displacement discontinuities [v] and [u], respectively.

We will first consider the opening mode of the crack. It is reasonable to assume that in the unloaded state (i.e., when $\sigma_y^* = 0$) the crack will be slightly open: $[v] = \Delta > 0$. In the closing mode we have $\sigma_y^* < 0$, and the required stress will increase rapidly as $[v] \to 0$. In fact we assume that an infinite flaw-plane stress σ_y^* is required to close the crack completely ([v] = 0) (i.e., to completely flatten out the roughness of the crack faces). The crack opening displacement cannot be negative since that would imply overlap of the crack faces. To open up the crack, $[v] > \Delta$, a slight resistance has to be overcome. The behavior described here can be represented by the relation

$$\sigma_{y}^{*} = T \frac{[v] - \Delta}{[v]} \tag{3}$$

Here T is the maximum tensile traction (very small) that can be transmitted across the crack faces. For an unbounded flaw plane the resistance to separation of the faces should decrease as $[v]-\Delta$ increases. This behavior is not represented by Eq. (3) since $\sigma_y^* \to T$ as $[v] \to \infty$. Thus, for that case Eq. (3) is not valid when $[v]-\Delta$ may assume large positive values. To model a

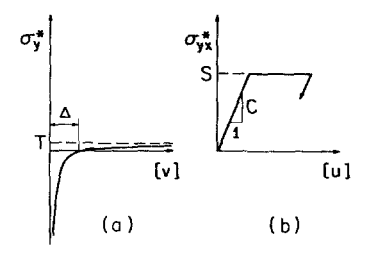


Fig. 2. Relations between averaged flaw-plane tractions σ_y^* and σ_{vx}^* , and averaged flaw-plane displacement separations [v] and [u].

crack, a residual resistance to separation of the crack faces is, however, a desirable feature since it may be thought of as representing the constraint on the crack-opening displacement by the presence of the crack tips. Equation (3) represents a nonlinear spring. The relation between σ_y^* and [v] is shown in Fig. 2 (a).

We have assumed that opening of the crack is independent of sliding of the crack faces. The opposite can, however, not be assumed. The resistance to sliding depends very much on the extent of crack opening, specifically on the magnitude of σ_y^* . When $\sigma_y^* > 0$ there will be very little resistance to sliding, while for $\sigma_y^* < 0$ there will be considerable resistance. A convenient relation between σ_{yx}^* and [u] is that we require $|\sigma_{yx}^*| \le S$, and

$$[\dot{u}] = \dot{\sigma}_{yx}^* / C \quad \text{for } |\sigma_{yx}^*| < S \tag{4}$$

The critical value S depends on σ_y^* . Here we assume the relation

$$S = S_o \exp(-\alpha \sigma_y^*) \tag{5}$$

Equation (5) satisfies the condition that S is small for $\sigma_y^* > 0$, while S increases rapidly as σ_y^* becomes negative (i.e. as the crack faces are pressed together).

With the arrival of a pulse at the flaw plane at t = 0, we have [u] = 0. As t increases Eq. (4) holds until [u]| = S/C. If $[\dot{u}]$ is non-zero at this point, the motion is altered abruptly to frictional sliding, in which σ_{yx}^* is equal to $S \operatorname{sgn}[\dot{u}]$. The frictional sliding ceases when $[\dot{u}]$ changes sign or when S exceeds C[[u]], say at $[u] = [u_1]$ and $\sigma_{yx}^* = S_1$. Equation (4) then takes over again in the form

$$\sigma_{vx}^* = C([u] - [u_1]) + S_1 \tag{6}$$

until a later time at which σ_{yx}^* again reaches the

critical value S. This occurs when

$$|\sigma_{yx}^*| = S, \qquad [\dot{u}] \neq 0 \tag{7}$$

A simple displacement history is illustrated in Fig. 2 (b). The key point to observe is the possibility of displacement hysteresis.

The parameters T, Δ , C, α and S_o have to be determined from the crack geometry and from experimental data.

In the next Section the reflection and transmission of plane pulses at an unbounded flaw plane will be investigated for arbitrary relations between tractions and displacement discontinuities at the flaw plane. The specific relations of Eqs. (3–7) will be applied in Section 5.

3. REFLECTION AND TRANSMISSION AT A FLAW PLANE

We will consider the reflection of an incident plane pulse at an unbounded flaw plane in an otherwise homogeneous unbounded solid. With reference to the coordinate system shown in Fig. 1 (b), the incident pulse is of the general form

$$\mathbf{u}^{in} = \mathbf{d}_{\alpha} f_{\alpha}^{i} (\xi_{\alpha} + \eta_{\alpha}) H(\xi_{\alpha} + \eta_{\alpha}), \qquad \alpha = L, T$$
(8)

where $\alpha = L$ and $\alpha = T$ define an incident longitudinal and transverse wave, respectively, and H() is the Heaviside step function. The unit vector \mathbf{d}_{α} defines the displacement direction:

$$\mathbf{d}_{L} = (\sin \theta_{L}, \cos \theta_{L}), \qquad \mathbf{d}_{T} = (\cos \theta_{T}, -\sin \theta_{T})$$
(9)

Also

$$\xi_{\alpha} = t - (x/c_{\alpha})\sin\theta_{\alpha}, \qquad \eta_{\alpha} = -(y/c_{\alpha})\cos\theta_{\alpha}$$
 (10)

where

$$c_L^2 = (\lambda + 2\mu)/\rho, \qquad c_T^2 = \mu/\rho$$
 (11)

Thus, the pulse arrives at x = 0, y = 0 at time t = 0.

The incident wave generates reflected and transmitted waves, which are indicated by \mathbf{u}^{re} and \mathbf{u}^{tr} , respectively. We may write

$$\mathbf{u}^{re} = \mathbf{d}_{L}^{r} f_{L}^{r} (\xi_{L}^{r} - \eta_{L}^{r}) + \mathbf{d}_{T}^{r} f_{T}^{r} (\xi_{T}^{r} - \eta_{T}^{r})$$
 (12)

$$\mathbf{u}^{tr} = \mathbf{d}_L^t f_L^t (\xi_L^t + \eta_L^t) + \mathbf{d}_T^t f_T^t (\xi_T^t + \eta_T^t)$$
 (13)

In (12) and (13)

$$\mathbf{d}_{L}^{r} = \left(\sin\theta_{L}^{r}, -\cos\theta_{L}^{r}\right), \qquad \mathbf{d}_{T}^{r} = \left(-\cos\theta_{T}^{r}, -\sin\theta_{T}^{r}\right)$$
(14)

$$\mathbf{d}_{L}^{t} = \left(\sin\theta_{L}^{t}, \cos\theta_{L}^{t}\right), \qquad \mathbf{d}_{T}^{t} = \left(\cos\theta_{T}^{t}, -\sin\theta_{T}^{t}\right)$$
(15)

$$\xi_{\beta}^{r} = t - (x/c_{\beta})\sin\theta_{\beta}^{r}, \qquad \eta_{\beta}^{r} = -(y/c_{\beta})\cos\theta_{\beta}^{r} \quad (16)$$

$$\xi_{\mathcal{B}}^{t} = t - (x/c_{\mathcal{B}})\sin\theta_{\mathcal{B}}^{t}, \qquad \eta_{\mathcal{B}}^{t} = -(y/c_{\mathcal{B}})\cos\theta_{\mathcal{B}}^{t} \quad (17)$$

where $\beta = L$, T. Here we have taken into account that the material is the same on both sides of the flaw plane.

The relations at the flaw plane are taken in the general form, discussed in Section 2. Thus, the stresses σ_y and σ_{yx} are continuous across the flaw plane, and these stresses are related to the displacement discontinuities [v] and [u] by specified relations.

The displacement discontinuities follow directly from (8) and (12)–(13). The relevant stresses follow by substituting \mathbf{u}^{in} , \mathbf{u}^{re} and \mathbf{u}^{tr} in

$$\sigma_{yx} = \mu \left(\frac{\partial u}{\partial y} + \frac{\partial v}{\partial x} \right) \tag{18}$$

$$\sigma_{y} = (\lambda + 2\mu) \left[\frac{\partial v}{\partial y} + (1 - 2/\kappa^{2}) \frac{\partial u}{\partial x} \right]$$
 (19)

where

$$\kappa^2 = c_L^2/c_T^2 = (\lambda + 2\mu)/\mu$$

The conditions on the flaw plane subsequently yield relations between $f_{\alpha}^{i}(\xi_{\alpha})$, $f_{\beta}^{r}(\xi_{\beta}^{r})$, $f_{\beta}^{t}(\xi_{\beta}^{r})$ ($\beta = L, T$), and the derivatives of these functions. Because of the infinite extent of the flaw plane, the functions $f_{\alpha}^{i}(\xi_{\alpha})$, $f_{\beta}^{r}(\xi_{\beta}^{r})$ and $f_{\beta}^{t}(\xi_{\beta}^{r})$ will have translational invariance with respect to their arguments, which implies that

$$\xi_I^r = \xi_T^r = \xi_I^t = \xi_T^t \equiv \xi_{\alpha} \tag{20}$$

By employing (16)–(17) it then follows from (20) that

$$(1/c_{\beta})\sin\theta_{\beta} = (1/c_{\alpha})\sin\theta_{\alpha} \tag{21}$$

which is Snell's law. In (21) we have left out the superscripts r and t, which are no longer required since $\theta_{\beta}^{t} = \theta_{\beta}^{r} = \theta_{\beta}$. We limit this paper to the case $(c_L/c_T)\sin\theta_T < 1$ (i.e., subcritical incidence of transverse waves).

By the use of (20) and (21) the displacement discontinuities can now be expressed as

$$[u] = \sin \theta_L [f_L^t(\xi_\alpha) - f_L^r(\xi_\alpha)]$$

$$+ \cos \theta_T [f_T^t(\xi_\alpha) + f_T^r(\xi_\alpha)] - f^i(\xi_\alpha) d_{\alpha x}$$
(22)

$$[v] = \cos \theta_L [f_L^t(\xi_\alpha) + f_L^r(\xi_\alpha)]$$
$$-\sin \theta_T [f_T^t(\xi_\alpha) - f_T^r(\xi_\alpha)] - f^i(\xi_\alpha) d_{\alpha y}$$
(23)

From continuity of $\sigma_{\nu x}$ it follows that

$$-C_{L\alpha}\dot{f}^{i}(\xi_{\alpha}) + \kappa^{-1}\sin 2\theta_{L}\dot{f}^{r}_{L}(\xi_{\alpha}) - \cos 2\theta_{T}\dot{f}^{r}_{T}(\xi_{\alpha})$$

$$= -\kappa^{-1}\sin 2\theta_{L}\dot{f}^{i}_{L}(\xi_{\alpha}) - \cos 2\theta_{T}\dot{f}^{i}_{T}(\xi_{\alpha})$$
(24)

where a dot denotes a derivative with respect to the argument, and

$$C_{LL} = \kappa^{-1} \sin 2\theta_L, \quad C_{LT} = \cos 2\theta_T$$
 (25)

Continuity of normal stress σ_{ν} yields

$$-C_{T\alpha}\dot{f}^{i}(\xi_{\alpha}) - \cos 2\theta_{T}\dot{f}_{L}^{r}(\xi_{\alpha}) - \kappa^{-1}\sin 2\theta_{T}\dot{f}_{T}^{r}(\xi_{\alpha})$$

$$= -\cos 2\theta_{T}\dot{f}_{L}^{i}(\xi_{\alpha}) + \kappa^{-1}\sin 2\theta_{T}\dot{f}_{T}^{i}(\xi)$$
(26)

where

$$C_{TL} = C_{LT}, \quad C_{TT} = -\kappa^{-1} \sin 2\theta_T \tag{27}$$

Equations (24) and (26) may now be integrated to yield

$$C_{LL}\Delta_L^+ + C_{LT}\Delta_T^- = C_{L\alpha}f^i(\xi_\alpha) \tag{28}$$

$$C_{LT}\Delta_L^- + C_{TT}\Delta_T^+ = C_{T\alpha}f^i(\xi_\alpha) \tag{29}$$

where

$$\Delta_{\alpha}^{\pm} = f_{\alpha}^{t}(\xi_{\alpha}) \pm f_{\alpha}^{r}(\xi_{\alpha}) \tag{30}$$

Equations (28) and (29) can be used to solve for $\Delta_L^-(\xi_\alpha)$ and $\Delta_T^-(\xi_\alpha)$. Substitution of the results in the expressions for [u] and [v], (22) and (23), yields

$$[u] = \cos \theta_T \left(\Delta_T^+ - f_\alpha^i \delta_{\alpha T} \right) / C_{LT}$$
 (31)

$$[v] = \cos \theta_L \left(\Delta_L^+ - f_\alpha^i \delta_{\alpha L} \right) / C_{LT}$$
 (32)

The stresses at the flaw plane at the side of transmitted waves may be written as

$$-\frac{2c_L}{\lambda + 2\mu}\sigma_y^* = C_{LT}(\dot{\Delta}_L^+ + \dot{\Delta}_L^-) + C_{TT}(\dot{\Delta}_T^+ + \dot{\Delta}_T^-)$$

$$-\frac{2c_T}{\mu}\sigma_{yx}^* = C_{LL}(\dot{\Delta}_L^+ + \dot{\Delta}_L^-) + C_{LT}(\dot{\Delta}_T^+ + \dot{\Delta}_T^-)$$

(34)

(33)

where, as before, a dot denotes differentiation with respect to the argument. We can next eliminate Δ_L^- and Δ_T^- from these expressions by using (28) and (29). Subsequent elimination of Δ_L^+ and Δ_T^+ by the use of (31) and (32) yields

$$-\frac{2}{\rho c_x} \sigma_y^* = \frac{D}{\cos \theta_x} [\dot{v}] + 2C_{T\alpha} \dot{f}_\alpha^i(\xi_\alpha) \qquad (35)$$

$$-\frac{2}{\rho c_x} \sigma_{yx}^* = \frac{D}{\cos \theta_x} [\dot{u}] + 2C_{L\alpha} \dot{f}_{\alpha}^i(\xi_{\alpha}) \qquad (36)$$

where

$$D = C_{LT}^2 - C_{LL}C_{TT} > 0 (37)$$

Substitution of (35) and (36) into the relations between σ_y^* , σ_{yz}^* and [u], [v] yields a set of inhomogeneous nonlinear ordinary differential equations for [u] and [v], which in general must be solved numerically.

Finally, the reflected and transmitted amplitudes are given in terms of [u] and [v] by

$$f_L^r(\xi) = \frac{1}{2} \left\langle \frac{C_{LT}}{\cos \theta_L} [v] + \frac{C_{TT}}{\cos \theta_T} [u] \right\rangle$$
 (38)

$$f_T^r(\xi) = \frac{1}{2} \left\langle \frac{C_{LL}}{\cos \theta_L} [v] + \frac{C_{LT}}{\cos \theta_T} [u] \right\rangle$$
 (39)

$$f_L^i(\xi) = \frac{1}{2} \left\langle \frac{C_{LT}}{\cos \theta_L} [v] - \frac{C_{TT}}{\cos \theta_T} [u] \right\rangle + \delta_{L\alpha} f_{\alpha}^i(\xi)$$
(40)

$$f_T^t(\xi) = \frac{1}{2} \left\langle \frac{C_{LT}}{\cos \theta_T} [u] - \frac{C_{LL}}{\cos \theta_L} [v] \right\rangle + \delta_{T\alpha} f_{\alpha}^i(\xi)$$
(41)

4. SPECULAR REFLECTION BY A FLAT CRACK

In this section we consider a flat crack as a flaw plane of finite dimensions with the reflection and transmission properties that have been discussed in Section 2. Under the influence of an incident wave the tractions are continuous across the faces of the crack, but the displacement components may suffer discontinuities. For a surface of displacement discontinuity in an unbounded body, the radiated elastodynamic field may be expressed in terms of a well-known representation integral (see e.g. [8, p. 103]). The representation integral employs the basic singular solution, which is the field generated by a point load per unit volume applied at position $\mathbf{x} = \boldsymbol{\zeta}$, and pointing in the x_k direction with time dependence g(t), i.e.,

$$f_i = \delta_{ik} g(t) \delta |\mathbf{x} - \boldsymbol{\zeta}| \tag{42}$$

The generated displacement field may be expressed in the form

$$4\pi\rho u_{i;k}^{G}(\mathbf{x},t;\zeta) = D_{i}^{k}\{\xi;g(t)\}$$
 (43)

where (see Ref. [8], Eq. (3.96))

$$D_{i}^{k}\{\xi;g(t)\} = \frac{1}{r} (3\hat{x}_{i}\hat{x}_{k} - \delta_{ik}) \int_{1/c_{L}}^{1/c_{T}} sg(t - rs) ds$$

$$+ \frac{\hat{x}_{i}\hat{x}_{k}}{r} \left[\frac{1}{c_{L}^{2}} g\left(t - \frac{r}{c_{L}}\right) - \frac{1}{c_{T}^{2}} g\left(t - \frac{r}{c_{T}}\right) \right]$$

$$+ \frac{\delta_{ik}}{c_{T}^{2}} \frac{1}{r} g\left(t - \frac{r}{c_{T}}\right)$$
(44)

In (44)

$$r = |\mathbf{x} - \boldsymbol{\zeta}|, \quad \hat{x}_i = (x_i - \boldsymbol{\zeta}_i)/r \tag{45}$$

Note that here we have taken the point load per unit volume, whereas in Ref. (8) it was taken per unit mass. Hence ρ does not appear in the right hand side of the corresponding expression in Ref. (8). The stress components follow from Hooke's Law:

$$4\pi\rho\tau_{ij;k}^{G}(\mathbf{x},t;\boldsymbol{\zeta}) = S_{ij}^{k}\{\boldsymbol{\zeta};g(t)\}$$
 (46)

where the operator $S_{ij}^{k}[\]$ is given by Eq. (3.98) of Ref. (8).

Now consider a surface A of displacement discontinuity $[u_i(\mathbf{x}, t)]$. It then follows from the representation integral given by Eq. (3.105) of Ref. (8) that

$$4\pi\rho u_k(\zeta,t) = \int_{\mathcal{A}} n_j S_{ij}^k \{\zeta; [u_i(\mathbf{x},t)]\} dA(\mathbf{x}) \quad (47)$$

where summations over the indices i and j are implied,

$$\left[u_i(\mathbf{x},t)\right] = u_i^+ - u_i^- \tag{48}$$

and **n** is the normal on the plus face of the surface A. Equation (47) simplifies substantially in the far field (i.e., when $r \gg |\mathbf{x}|$). It can then be shown that

$$D_i^k\{\zeta; g(t)\} \simeq \frac{\hat{x}_i \hat{x}_k}{r} \frac{1}{c_L^2} g\left(t - \frac{r}{c_L}\right) + \frac{1}{r} \left(\delta_{ik} - \hat{x}_i \hat{x}_k\right) \frac{1}{c_T^2} g\left(t - \frac{r}{c_T}\right)$$

$$(49)$$

provided that g(s) = O(1) for s = O(1) and g(s) = o(1/r) for s = O(r). The corresponding stress is then obtained as

$$\tau_{ij;k}^G \cong \tau_{ij;k}^{G,L} + \tau_{ij;k}^{G,T} \tag{50}$$

where

$$\tau_{ij;k}^{G,\alpha} = -\frac{1}{c_{\alpha}} B_{ij;k}^{G,\alpha} \frac{1}{4\pi r} \dot{g} \left(t - \frac{r}{c_{\alpha}} \right), \alpha = L, T$$
 (51)

$$B_{ij;k}^{G,L} = (2\hat{x}_i\hat{x}_j\kappa^{-2} + \delta_{ij}(1 - 2\kappa^{-2}))\hat{x}_k$$
 (52)

$$B_{ij:k}^{G,T} = \delta_{ik}\hat{x}_i + \delta_{jk}\hat{x}_i - 2\hat{x}_i\hat{x}_j\hat{x}_k \tag{53}$$

and

$$r \cong |\mathbf{x}| - (\hat{\mathbf{x}} \cdot \boldsymbol{\zeta}), \, \hat{\mathbf{x}} = \mathbf{x}/|\mathbf{x}| \tag{54}$$

Equation (50) reduces to the corresponding expression for a time-harmonic force, given as Eqs. (1.64)–(1.68) in Ref. (9), by the substitution $g(t - r/c_{\alpha}) = \exp[-i\omega(t - r/c_{\alpha})]$, where $\omega = k_{\alpha}c_{\alpha}$.

Substitution on (50) in (47) yields in the far field

$$u_{k}(\mathbf{x},t) = -\frac{1}{4\pi R} \sum_{\beta=I,T} \frac{1}{c_{\beta}} B_{ij;k}^{G,\beta} n_{j} U_{i}^{\beta}(t,R) \quad (55)$$

where

$$U_{i}^{\beta}(t,R) = \int_{A} \left[\dot{u}_{i} \left(\xi, t - \frac{R}{c_{\beta}} + \frac{1}{c_{\beta}} \hat{\mathbf{x}} \cdot \xi \right) \right] dA(\xi)$$
(56)

For convenience we have taken the origin in the plane of the crack, R = |x|, and ζ and x have been interchanged.

Equation (55) would give the radiated field if the crack-opening displacement were known a priori. This is, however, not the case. In an actual scattering problem the crack-opening displacement is part of the solution being sought. It is, however, possible to obtain an approximate solution to the scattering problem by making a judicious a priori estimate of $[u_i]$. A simple and useful estimate, which has validity at higher frequencies, is obtained by assuming that $[u_i]$ is the same as for an infinite flaw plane. This approximation ignores the effect of the crack edge on the crack-opening displacement.

The value of $[u_i]$ for an infinite flaw plane follows from the results of Section 3. Let the vector \mathbf{p}_{α} be in the incident wave direction and $|\mathbf{p}_{\alpha}| = 1/c_{\alpha}$. Then $[\mathbf{u}] = [\mathbf{u}(t - \mathbf{p}_{\alpha} \cdot \boldsymbol{\zeta})]$. We also define the vector \mathbf{q}_{β} in the scattered wave direction by $\hat{\mathbf{x}} = \mathbf{q}_{\beta}c_{\beta}$, and thus $|\mathbf{q}_{\beta}| = 1/c_{\beta}$. Then we may write

$$\left[u_{i}\left(\boldsymbol{\zeta}, t - \frac{R}{c_{\beta}} + \frac{1}{c_{\beta}}\hat{\mathbf{x}}\cdot\boldsymbol{\zeta}\right)\right]$$

$$\equiv \left[\dot{u}_{i}\left(t - \frac{R}{c_{\beta}} + (\mathbf{q}_{\beta} - \mathbf{p}_{\alpha})\cdot\boldsymbol{\zeta}\right)\right]$$
(57)

Now, consider the integral

$$I = \int_{A} \dot{f}(\mathbf{a} \cdot \mathbf{\zeta}) \, dA(\mathbf{\zeta}) \tag{58}$$

Let us define the new crack-plane coordinates ξ , η by

$$\zeta = \xi \frac{\mathbf{n} \wedge (\mathbf{a} \wedge \mathbf{n})}{|\mathbf{n} \wedge \mathbf{a}|} + \eta \frac{\mathbf{n} \wedge \mathbf{a}}{|\mathbf{n} \wedge \mathbf{a}|}$$
 (59)

Thus

$$\mathbf{a} \cdot \mathbf{\zeta} = |\mathbf{n} \wedge \mathbf{a}| \mathbf{\xi} \tag{60}$$

and

$$I = \int_{\mathcal{A}} \dot{f}(|\mathbf{n} \wedge \mathbf{a}|\xi) \, d\xi \, d\eta$$
$$= \int_{\partial \mathcal{A}} f(\mathbf{a} \cdot \xi) \frac{\mathbf{n} \wedge \mathbf{a}}{|\mathbf{n} \wedge \mathbf{a}|^2} \cdot d\xi \tag{61}$$

where ∂A is the edge of the crack. By identifying $\mathbf{a} = \mathbf{q}_{\beta} - \mathbf{p}_{\alpha}$, we can then write (56) as

$$U_{i}^{\beta}(t,R) = \int_{\partial A} \left[u_{i} \left(t - \frac{R}{c_{\beta}} + (\mathbf{q}_{\beta} - \mathbf{p}_{\alpha}) \cdot \zeta \right) \right] \times \frac{\mathbf{n} \wedge (\mathbf{q}_{\beta} - \mathbf{p}_{\alpha})}{|\mathbf{n} \wedge (\mathbf{q}_{\beta} - \mathbf{p}_{\alpha})|^{2}} \cdot d\zeta$$
 (62)

Note that the edge integral is taken in the counterclockwise sense.

Equation (62) has been derived for arbitrary angles of observation. Comparisons with exact solutions for analogous problems have, however, indicated that the approximation gives the best results in the shadow zones and in the zones of specular reflection. In these zones we have either $\mathbf{q}_{\beta} - \mathbf{p}_{\alpha} = 0$ or $(\mathbf{q}_{\beta} - \mathbf{p}_{\alpha})$ is normal to the plane of the crack, and hence $(\mathbf{q}_{\beta} - \mathbf{p}_{\alpha}) \cdot \zeta$ vanishes. Substitution of this result in (57) and (56) yields

$$U_i^{\beta}(t,R) = A[\dot{u}_i](t - R/c_{\beta})^{-1} \tag{63}$$

where A is the area of the crack face, and we have used the notation

$$\left[\dot{u}_i(t-R/c_\beta)\right] = \left[\dot{u}_i\right](t-R/c_\beta) \tag{64}$$

Thus the discontinuity in the particle velocity across the crack faces, computed at the origin, radiates as a spherical wave.

Let the crack lie in the plane y = 0. The crack normal **n** is then equal to \mathbf{i}_2 . If the incident wave motion is in the plane of x and y, then the scattered longitudinal and transverse fields in the specular and

shadow directions are

$$\mathbf{u}^{L}(\mathbf{x},t) = \frac{-A}{4\pi R c_{L}} \left\{ \mp \kappa^{-2} \sin 2\theta_{L} [\dot{u}] \right\}$$

$$+ \cos 2\theta_{T} [\dot{v}] \left\{ (t - R/c_{L}) \right\} \left\{ \mathbf{d}_{L}^{\prime} \right\}$$

$$\mathbf{u}^{T}(\mathbf{x},t) = \frac{-A}{4\pi R c_{T}} \left\{ \cos 2\theta_{T} [\dot{u}] \right\}$$

$$\pm \sin 2\theta_{T} [\dot{v}] \left\{ (t - R/c_{T}) \right\} \left\{ \mathbf{d}_{T}^{\prime} \right\}$$

$$\mathbf{d}_{T}^{\prime}$$

$$(66)$$

u and v are the displacement components in the x and y directions, the notation defined by (64) has been used, and the displacement vectors for the reflection and shadow fields (superscripts r and t, respectively) are given in Eqs. (14) and (15).

It is of interest to compute the reflection and shadow fields when the crack faces are stress free $(\sigma_y^* = \sigma_{yx}^* = 0)$. The reflected field of type β due to an incident wave of type α is found to be

$$\mathbf{u}^{\beta}(\mathbf{x},t) = \frac{A}{2\pi R} \frac{\cos\theta_{\beta}}{c_{\beta}} R_{\beta}^{\alpha} \dot{f}_{\alpha}^{i}(t - R/c_{\beta}) \mathbf{d}_{\beta}^{r}$$
 (67)

where R^{α}_{β} are the reflection coefficients from a traction free surface

$$R_{\beta}^{\alpha} \equiv \begin{cases} \left(C_{LT}^{2} + C_{LL}C_{TT} \right) / D, & \beta = \alpha \\ 2C_{\alpha\alpha}C_{LT} / D, & \beta \neq \alpha \end{cases}$$
 (68)

The shadow fields are found to be zero when $\beta \neq \alpha$, and when $\beta = \alpha$ they are

$$\mathbf{u}^{\alpha}(\mathbf{x},t) = \frac{A}{2\pi R} \frac{\cos\theta_{\alpha}}{c_{\alpha}} \dot{f}_{\alpha}^{i}(t - R/c_{\alpha}) \mathbf{d}_{\alpha}^{t}$$
 (69)

Now consider the case when the crack faces do interact and transmit tractions. Let $\mathbf{u}_{o}^{\beta,r}$ and $\mathbf{u}_{o}^{\beta,t}$, $\beta = L, T$ be the reflected and shadow fields for the stress-free crack, defined by Eqs. (67) and (69), respectively. The corresponding fields in the presence of tractions follow from Eqs. (65), (66), (35), and (36) as

$$\mathbf{u}^{L}(\mathbf{x},t) = \mathbf{u}_{o}^{L, \{'_{t}\}} + \frac{A\cos\theta_{L}}{2\pi R\rho c_{L}^{2}D}$$

$$\times \left\{ C_{LT}\sigma_{v}^{*} \pm \kappa C_{TT}\sigma_{vx}^{*} \right\} (t - R/c_{L})\mathbf{d}_{L}^{\{'_{t}\}}$$
(70)

$$\mathbf{u}^{T}(\mathbf{x},t) = \mathbf{u}_{o}^{T,\left\{r\right\}} + \frac{A\cos\theta_{T}}{2\pi R\rho c_{T}^{2}D}$$

$$\times \left\{ \pm \kappa^{-1}C_{LL}\sigma_{y}^{*} + C_{LT}\sigma_{yx}^{*} \right\} (t - R/c_{T})\mathbf{d}_{T}^{r}$$
(71)

where the notation $\sigma_y^*(t - R/c_\beta)$ and $\sigma_{yx}^*(t - R/c_\beta)$ is analogous to (64).

5. NUMERICAL RESULTS AND DISCUSSION

In this Section we apply the general results of Sections 3 and 4 with the interface stresses σ_y^* and σ_{yx}^* as given in Section 2. In all the numerical examples we have taken the following values of the parameters in Eqs. (3)–(5)

$$\Delta = .5, \quad T = .1\mu, \quad C = \mu/\Delta$$

$$S_o = .3\mu, \quad \alpha = 15/\mu, \tag{72}$$

where Δ and all subsequent displacements are normalized with respect to the maximum displacement of the incident pulse, which is of magnitude unity. A Poisson's ratio of 1/3 is taken. The results for this choice of parameters illustrate the salient features of the model. Other parameters have been considered, but the corresponding results do not add much to the understanding of the problem, and they will not be discussed here. The shape of the incident profile f_{α}^{i} is the same in all examples, and is shown in Fig. 3(a).

We first consider the pulse of finite duration incident upon an unbounded flaw plane. If the incident pulse is of type α , $\alpha = L, T$ then the displacements u^+, v^+ and u^-, v^- on the upper and lower faces follow from Section 3 as

$$u^{\pm} = \pm \frac{1}{2} [u] - ([v] - \Delta) \frac{\sin(2\theta_T - \theta_L)}{2\cos\theta_L}$$

$$+ (\sin\theta_L \delta_{L\alpha} + \cos\theta_T \delta_{T\alpha}) f_{\alpha}^{i} \qquad (73)$$

$$v^{\pm} = \pm \frac{1}{2} [v] + [u] \frac{\sin(2\theta_T - \theta_L)}{2\kappa\cos\theta_T}$$

$$+ (\cos\theta_L \delta_{L\alpha} - \sin\theta_T \delta_{T\alpha}) f_{\alpha}^{i} \qquad (74)$$

The displacements v^{\pm} and u^{\pm} are shown in Figs. 3(b) and 3(c) for normally incident L and T waves,

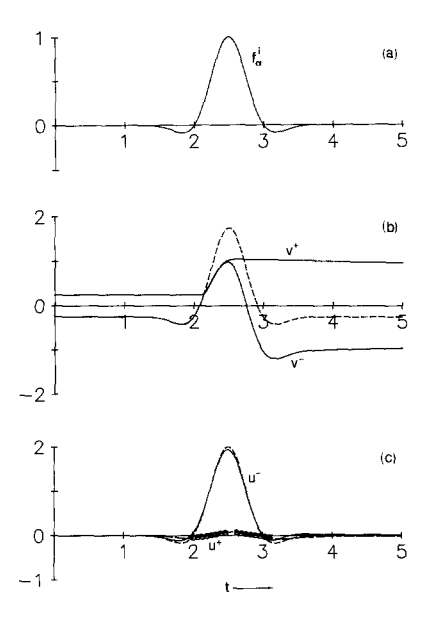


Fig. 3. (a) Profile of the incident pulse. (b) Displacements v^+ and v^- for an L-wave normally incident on the flaw plane. The dashed line is v^- in the absence of flaw-plane tractions. (c) Displacements u^+ and u^- for a normally incident T-wave. The circles indicate the regions of frictional sliding, and the short-dashed line represents u^- for a traction-free plane.

respectively. We have also plotted the displacements u^- and v^- for the stress free interface defined by $\sigma_v^* = \sigma_{vx}^* = 0$. Figure 3(b) shows that v^- is the same as for a stress-free interface until the two faces become very close together. The resistance to closing then becomes very large, causing the upper face to lift. When the pulse has passed through, and the lower face recedes, the large pressure on the two faces changes to a small tension which slowly brings the two faces back to their equilibrium positions. The decay rate in our example is exceedingly slow, leaving the flaw plane open for a long time after the passage of the pulse. In Fig. 3(c) we note how the shear stress in the flaw plane causes the upper face to move in phase with the lower one, though the magnitude of u^+ is much smaller. The transfer of energy leaves $u^$ slightly smaller than the stress-free u^- . The times at which the flaw-plane sliding is in the frictional regime (see Eq. (6)) are indicated by the circles on the u^+ curve.

For the same pulse profile, the displacements due to T waves incident at $\pm 20^{\circ}$ are plotted in Fig. 4. For an angle of incidence of $+20^{\circ}$ the pulse causes the gap to open while it closes for -20° . In Fig. 4(d) we see how the flaw-plane closure affects the shear stress. As the faces close, the resistance to sliding is

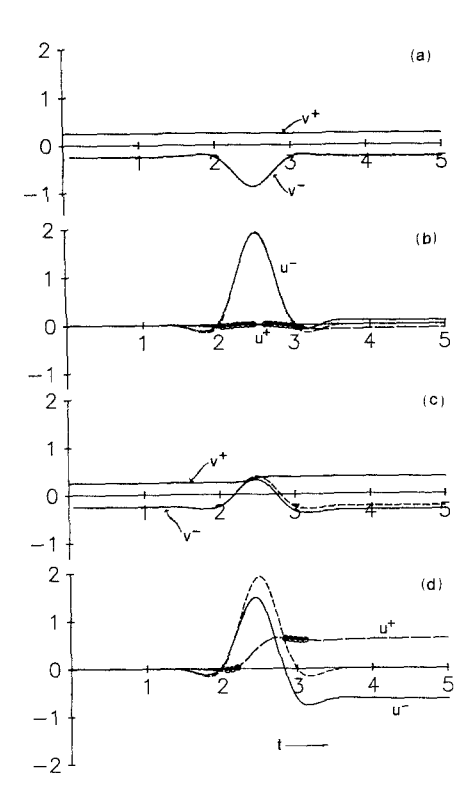


Fig. 4. Vertical (a) and horizontal (b) displacements on the flaw plane for a T-wave incident at 20° . (c) and (d) are for T-wave incidence at -20° .

governed mainly by Eq. (4), causing the upper face to move significantly. When the faces open, the critical stress S of Eq. (5) is decreased, allowing frictional sliding to take place. The net effect after the pulse has passed through is to leave the faces horizontally displaced relative to one another.

Figure 5 shows the reflected and transmitted fields for the T wave incident at -20° . The stress-free results are shown for comparison. We note that there are no transmitted waves for the stress-free interface.

The reflected and transmitted waves are shown in Fig. 6 for an L wave incident at 20°. The step-like transmitted L wave of Fig. 6(c) is particularly interesting.

We now consider the incidence of pulses on flaw planes of finite area (cracks). We shall only be interested in the specularly reflected and transmitted fields, therefore the results of Eqs. (65) and (66) are applicable. In all the examples, the quantities plotted are for $\beta = L, T$.

$$U_{\beta^t}^r \equiv \frac{R}{A} \mathbf{u}^{\beta} \cdot \mathbf{d}_{\beta^t}^r \tag{75}$$

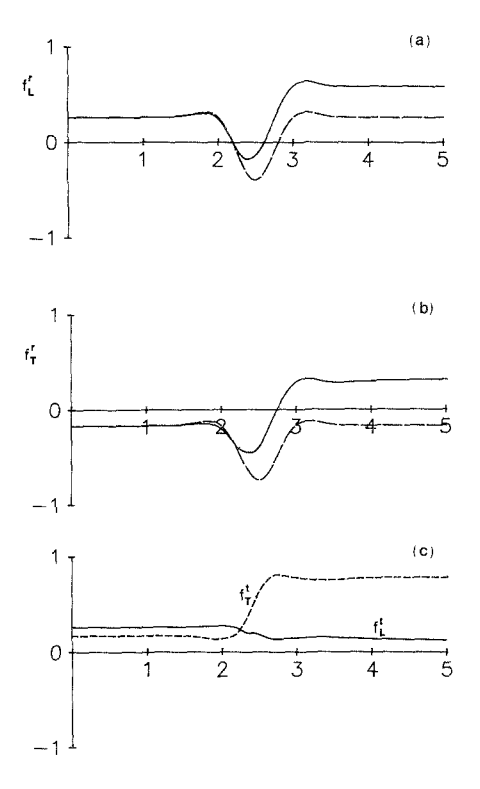


Fig. 5. T-wave incident at -20° (a) Reflected L-wave, (b) reflected T-wave. The dashed lines in (a) and (b) are for the traction-free plane. (c) Transmitted L and T-waves.

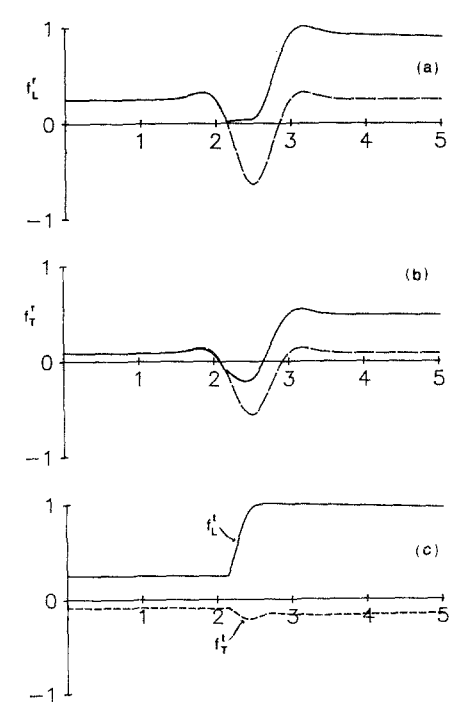


Fig. 6. L-wave incident at 20°. Reflected (a), (b), and transmitted waves (c).

where the various quantities on the right-hand side of Eq. (75) are defined in Section 4. Thus, U_{β}^{r} and U_{β}^{t} are independent of the crack size and shape and of the observation distance R.

Normal incidence of L and T waves is considered in Fig. 7. In both cases there are no mode conversions and the reflected and transmitted fields are identical. The fields produced by a stress-free crack are shown for comparison. The results are basically proportional to the time derivatives of the displacement discontinuities across the infinite flaw plane. It is useful to compare Fig. 7 with Fig. 3. In particular, the step-like jump in Fig. 7(a) is related to the rapid closure of the interface gap. It is noted that the tension part of the reflected pulse is affected by crack closure, while the compressive part is not.

The reflected and transmitted fields for L incidence at 20° are shown in Fig. 8. A novel feature, in comparison with the stress-free crack, is the appearance of a transmitted or "shadow" mode-converted T wave. These results should be compared with those of Fig. 6.

Shear-wave incidence also produces a mode-converted transmitted L wave, as is shown in Fig. 9 for T wave incidence at -20° . The induced crack closure also affects the reflected and transmitted T waves significantly. Similar computations for T incidence at 20° show little difference from the stress-free results, as expected from Fig. 5.

In summary, crack closure and the resistance to relative sliding of the crack faces have been modeled

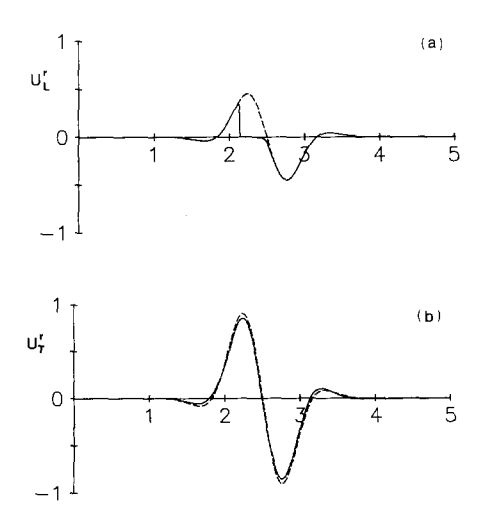


Fig. 7. Specularly reflected far-field amplitudes for normally incident L (a), and T-waves (b), on a crack. The results for the traction-free crack are indicated by the dashed lines.

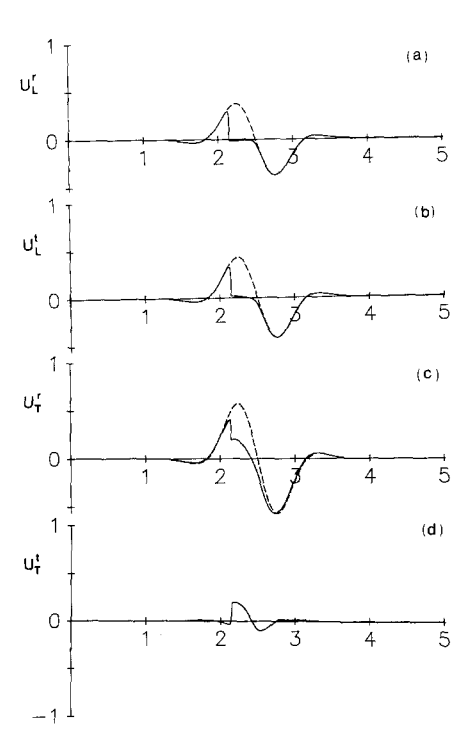


Fig. 8. L-wave incident on a crack at 20°. Reflected (a) and transmitted (b) L-wave amplitudes. Reflected (c) and transmitted (d) T-waves. Results for the traction-free crack are shown by dashed lines.

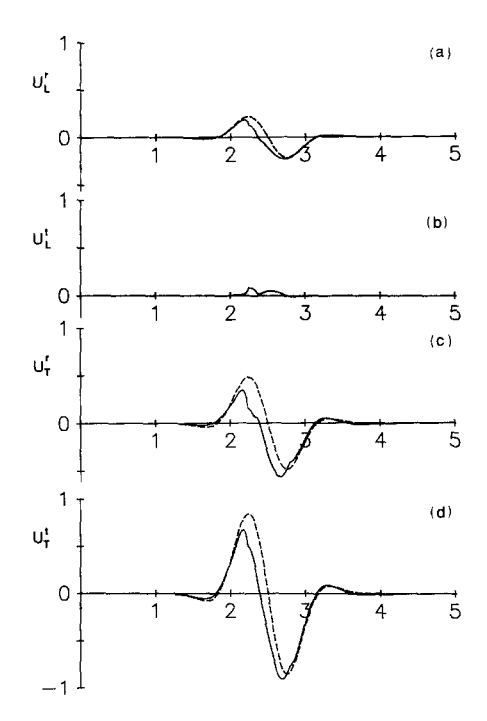


Fig. 9. Same as Fig. 8, except for a T-wave incident at -20° .

to investigate the influence of crack-face interaction on the scattered fields. Approximate results for the scattered fields in the zones of specular reflection and specular transmission show that crack-face interaction can be a significant effect. As might be expected the effect on the scattered fields is particularly noticeable if the incident pulse creates a significant interface pressure across the crack faces. This will happen for incident pressure pulses, but also for incident transverse waves when the displacement component normal to the crack, points towards the crack faces. The latter case was illustrated by considering a T-wave incident under an angle of incidence of -20° . When crack-face interaction is initiated by the incident pulse, part of the pulse is transmitted across the crack faces, and the reflected signal is correspondingly reduced. For non-interacting crack faces (zero crack-face tractions) the reflected displacement signal is proportional to the derivative of the incident pulse in the present approximation. For a compressive incident pulse the tension part of the reflected pulse may be significantly affected by crack-face interaction, while the compressive part will not be.

ACKNOWLEDGMENT

The work reported here was carried out under Contract DE-AC02-83ER13036.A000, with the De-

partment of Energy, Office of Basic Energy Sciences, Engineering Research Program.

REFERENCES

- N. F. Haines, The theory of sound transmission and reflection at contacting surfaces, Report RD/B/N4711, (Central Electricity Generating Board, Research Division, Berkeley Nuclear Laboratories, Berkeley, England, 1980).
- 2. R. B. Thompson, C. J. Fiedler, and O. Buck, Inference of fatigue crack closure stresses from ultrasonic transmission measurements, *Proc. Nondestructive Methods for Material Property Determination* (April 6–8, 1983, Hershey, PA, Plenum Press, New York, in press).
- 3. O. Buck, B. J. Skillings, and L. K. Reed, Simulation of closure: Effects on crack detection probability and stress distributions, in *Review of Progress in Quantitative Nondestructive Evaluation* 2, D. O. Thompson and D. E. Chimenti, eds. (Plenum Press, New York, in press).
- A. B. Wooldridge, The effects of compressive stress on the ultrasonic response of steel-steel interfaces and of fatigue cracks, Report NW/SSD/RR/42/79, (Central Electricity Generating Board, Northwestern Region, Manchester, England, 1979).
- A. B. Wooldridge, The effects of compressive stress and contaminating liquids on the ultrasonic detection of fatigue cracks, Revue du Cethedec, 17e annee, 4e trimestre 1980-NS80-2, 233-244 (1980).
- S. Golan, Measuring of closure forces with ultrasonic diffracted waves, in *New Procedures in Nondestructive Testing*, P. Höller, ed. (Springer Verlag, 1983).
- J. M. Richardson, Harmonic generation at an unbounded interface-I. Planar interface between semi-infinite elastic media, *Int. J. Engng. Sc.* 17:73-85 (1979).
- 8. J. D. Achenbach, Wave Propagation in Elastic Solids, (North-Holland/American Elsevier, Amsterdam, New York, 1973)
- J. D. Achenbach, A. K. Gautesen, and H. McMaken, Ray Methods for Waves in Elastic Solids-with Applications to Scattering by Cracks (Pitman Publ., London, 1982).